Talanta 201 (2019) 185–193

Contents lists available at ScienceDirect

Talanta

journal homepage: www.elsevier.com/locate/talanta

Phthalocyanine-doped polystyrene fluorescent nanocomposite as a highly selective biosensor for quantitative determination of cancer antigen 125

M.S. Attia[a,b,*], K. Ali[a], Maged El-Kemary[c], W.M. Darwish[d,**]

[a] Chemistry Department, Faculty of Science, University of Jeddah, P.O. Box 80327, Jeddah, 21589, Saudi Arabia
[b] Chemistry Department, Faculty of Science, Ain Shams University, Abbassia, 11566, Cairo, Egypt
[c] Institute of Nanoscience and Nanotechnology, Kafrelsheikh University, Egypt
[d] Department of Polymers and Pigments, National Research Centre, Elbohooth Street, Dokki, 12622, Giza, Egypt

ARTICLE INFO

Keywords:
Cancer antigen 125
Ni-phthalocyanine
Polymer
Quenching
Ovarian cancer
Luminescence intensity

ABSTRACT

A novel, simple, sensitive, and precise spectrofluorometric assay of cancer antigen [CA 125] is described. This modality is based on monitoring the quenching of the luminescence intensity at 790 nm of the phthalocyanine fluorophore, in a nanocomposite comprising the fluorophore and cationic polystyrene, which results from interaction with CA 125. The remarkable quenching of the luminescence intensity of the Ni-phthalocyanine complex doped in PS matrix by various concentrations of CA 125 was successfully utilized as an optical sensor for the determination of CA 125 in different serum samples of ovarian disease. The performance of the designed biosensor is determined through monitoring the quenching of the luminescence intensity at 790 nm by cancer antigen 125 after excitation at 685 nm, pH 7.3 in water. The calibration plot was achieved over the concentration range 1.0×10^{-2} – 127 U mL^{-1} CA-125 with a correlation coefficient of 0.99 and detection limit of 1.0×10^{-4} U mL^{-1}. The mechanism of the interaction between the nano thin film nickel(II)phthalocyanine and CA-125 was discussed. A significant correlation between the proposed method for the assessment of CA 125 and the standard method was applied to patients and controls.

1. Introduction

CA-125 (cancer antigen 125) is a surface antigen associated with non-mucinous epithelial ovarian cancer [1]. The protein is sloughed or secreted from the surface of the ovarian cancer cells into the serum or ascites [2]. The antigen reacts to a murine monoclonal antibody, OC 125 that was originally developed by immunizing mice with cells from ovarian cancer cell line OVCA 433 [3]. CA-125 antigen is the largest member of the mucin family of glycoproteins. It is a highly glycosylated protein and contains ~22.000 amino acids. The amphiphilic nature arises from the weakly hydrophobic domains close to the membrane and the polar glycosylated tail [4]. CA-125 test is not recommended for women with average OC risk. However, for the women with advanced OC, this test is the most potential test for detection of OC. This due to the fact that more than 90% of women with advanced OC have elevated CA-125 blood levels [5]. This is actually because ambiguous positive test results afford further invasive and unnecessary medical treatments [5]. It was observed that majority of women with late stage OC display significantly elevated CA-125 blood levels. Therefore, monitoring of these levels, in addition to certain physical signs are mostly applied for detection of OC [6]. Further, observing CA-125 blood levels during the therapeutic course is valuable for determining the response of the patient to the treatment [7] and for predicting a patient's prognosis after treatment [8]. In some cases, elevated CA-125 levels within individuals might be a strong indication to recurrence of OC [9]. The main two aspects of an efficient sensor are sensitivity and selectivity. These two parameters must be optimized in the development of an ideal sensor. It is noteworthy to mention that sensors should display a detectable signal and the change of signal by the sensor. As in many fields, nanotechnology contributes to production of advanced sensor materials with enhanced signal response. Phthalocyanines (Pcs), a great family of macrocyclic compounds, have recently found many industrial and medical applications due to their unique chemical and physical properties. The optical properties (absorption, fluorescence, photodynamics, photoconductivity) of Pcs arise from their chemical structure as a planar macrocycle containing 18 π electron arranged in a highly conjugated system [10]. Fluorescence is an important phenomenon of Pcs and has recently found many applications in the field of biomedical

* Corresponding author. Chemistry Department, Faculty of Science, University of Jeddah, P.O. Box 80327, Jeddah, 21589, Saudi Arabia.
** Corresponding author.
E-mail addresses: mohd_mostafa@sci.asu.edu.eg, Mohamed_sam@yahoo.com (M.S. Attia), waeldarwish78@yahoo.com (W.M. Darwish).

https://doi.org/10.1016/j.talanta.2019.03.119
Received 15 February 2019; Received in revised form 28 March 2019; Accepted 30 March 2019
Available online 04 April 2019
0039-9140/

sensors and fluorescence imaging [11]. However, most of Pcs absorb and emit in the far red region light spectrum and only few Pcs that function in the near infrared (NIR) region. Phthalocyanine-polystyrene films are known for good photochemical and photophysical properties and are applicable as fluorescence gas sensors [12] and in photocatalysis [13]. Fluorescent polystyrene microspheres embedded with acridine orange and rhodamine 101 were prepared by gradual solvent evaporation method. In this work, a near infrared-fluorescent phthalocyanine was synthesized as a NIR fluorescent dye and embedded in polystyrene matrix affording a monolithic and highly fluorescent polymer thin film. Thin film was prepared as a medical kit, not just as a sensor, for quantitative determination of CA-125 in different serum samples of the ovarian cancer disease. The assessment process depends on the quenching of the luminescence intensity of the optical biosensor by various concentrations of CA-125 at 790 nm after excitation at 685 nm in water.

2. Experimental

2.1. Methods

All manipulations were carried out under argon stream, dried over P_2O_5, using standard Schlenk line technique. All fluorescence measurements were recorded with a Meslo-PN (222-263,000) Thermo Scientific Lumina fluorescence Spectrometer. The absorption spectra are recorded with Thermo UV–Visible double-beam spectrophotometer. All pH measurements are made with a pHs-Janway3040 ion analyzer. The TEM image of the nano Ni-phthalocyanine complex optical sensor doped in polymeric matrix was measured (19.4 ± 0.7 nm) by using the JEOL JEM-1230. The morphology of the optical sensor was studied using AFM recorded using Park XE 15. X-Ray Diffraction patterns (XRD) were measured using a Philips Analytical, X'Pert PRO. The IR spectra (4000-400 cm^{-1}) were measured at room temperature with Jasco FT/IR-6100 type A. LCQ-Mass-Spectra were recorded on Thermo Finnigan (LCQ Advantage Max) Ion Trap using MeOH/THF mixture as solvent. Analysis of carbon, hydrogen and nitrogen was performed by combustion of the samples at 1150 °C in a Vario Elementar EL instrument. Determination of nickel in Ni(II)*Pc* **2** was achieved using a double beam flame atomic absorption (Varian Spectra A-220) equipped with cross flow nebulizer after decomposition of the samples by heating in nitric acid.

Dynamic light scattering (DLS) and Zeta potential measurements were carried out using PSS instrument, using the 632 nm line of a He-Ne laser as the incident light with angel 90° and Zeta potential with external angel 18.9°. GPC measurements of polystyrene were carried out using Agilent 1100 series, gel permeation chromatography with refractive index detector using THF as an eluent and calibrated PL 5 μm, (100, 104, 105 Å) on series of columns against polystyrene standard.

2.2. Materials

Dimethylformamide (DMF) and 1-pentanol were distilled under reduced pressure before use. 2,3-Dicyanohydroquinone (DCHQ); 2-ethylhexyl bromide; anhydrous potassium carbonate K_2CO_3 were purchased from WINLAB UK. Nickel acetate Ni(II)Ac.$4H_2O$, DBU, NaH_2PO_4, NaOH, NaCl, KCl, albumin, uric acid, urea, triglyceride, Polyvinylpyrrolidone (PVP, MW = 40,000) and glucose were purchased from Sigma-Aldrich Chemical Co. Styrene monomer (> 99%; Merck, Darmstadt, Germany) was distilled to remove the inhibitor in vacuum and stored at 4 °C until use.

The initiator, α,α′-azodiisobutyramidinedihydrochloride (AIBA), was purchased from Fluka (USA) and used as received. Cancer antigen 125 (CA-125, 140 U mL^{-1}), CA 19-9 (Carbohydrate antigen 19-9, 130 U mL^{-1}), CA 15-3 (Carcinoma antigen, 130 U mL^{-1}) and CEA (Carcinoembryonic antigen, 130 U mL^{-1}) were purchased from (orb 98857, Biorbyt), the working solutions of CA-125 and other biomarkers were prepared by dissolving the vial content of the biomarker in 1 mL water. The phosphate buffer of pH 7.3 was prepared by mixing 100 mL of 0.1 mol L^{-1} NaH_2PO_4 with 58.2 mL of 0.1 mol L^{-1}NaOH and volume is completed to 200 mL by distilled water. The validity and selectivity of the developed method was tested by studying the influence of a series of interfering species e.g. CEA (130 U mL^{-1}), CA 19-9(130 U mL^{-1}), CA 15-3 (130 U mL^{-1}), NaCl, KCl (2.0×10^{-3} mol L^{-1}), albumin (0.7 g L^{-1}), uric acid (0.08 g L^{-1}), urea (0.06 g L^{-1}), total protein (0.01 g L^{-1}), (0.06 g L^{-1}) triglyceride and glucose (0.08 g L^{-1}) on the luminescence spectrum of the thin film NiPc **2** doped PS matrix after addition of CA-125 (130 U mL^{-1}). The presence of CEA, CA 19-9 and CA 15-3 in combination with CA-125 in the serum sample of ovarian cancer disease is considered a major problem in the assessment of CA-125 in the serum sample. To solve this problem, we add the CA-125 in the serum sample of patient to the micro plate coated by an antibody of CA-125 followed by washing by phosphate buffer to obtain the CA-125 only. Then the luminescence intensity of the optical biosensor was calculated in absence and in presence of the CA 125 obtained from the washing process. The ΔF was calculated to compare the between the interaction of CA 125 and the different interfering species with the optical biosensor (ΔF is the luminescence intensity of the optical sensor in absence of the interfering species – the luminescence intensity of the optical sensor in presence of the interfering species). Human samples were obtained from the New Al-Kasr-EL-Aini Teaching Hospital Cairo University and Ain Shams Specialized Hospital, Ain shams University, Cairo, Egypt in accordance with WHO (World Health Organization) approved protocol for human specimen collection and for the use of this material and related clinical information for research purposes. All patients consented and approved the using of their clinical samples in the research work.

2.3. Synthesis and characterization

2.3.1. Synthesis of 1,2-Dicyano-3,6-bis(2-ethylhexyloxy)benzene 1

A mixture of 2,3-Dicyano-1,4-hydroquinone (DCHQ) (1.28 g, 8 mmol) and 2-ethylhexyl bromide (3.48 g, 18 mmol) was dissolved in 25 mL of dry DMF and then potassium carbonate (2.21 g, 16 mmol) was slowly added. The mixture was heated at 50 °C under static argon for 16 h. After cooling, the reaction mixture was poured on 30 mL of deionized water and the produced buff precipitate was filtered off. The solid was dissolved in chloroform and filtered to remove the unreacted DCHQ. After drying over anhydrous $CaCl_2$, chloroform was at room temperature under reduced pressure to afford greenish yellow microcrystals of **1** (m.p. 47-48 °C). Yield = 2.5 g, 81%. MS (EI, 70eV): *m/z* 384.8 $(M)^+$.Anal. Calc. for $C_{24}H_{36}N_2O_2$: C, 74.96; H, 9.44; N, 7.28. Found: C, 74.21; H, 10.24; N, 6.57. IR (KBr pellets) ν_{max} (cm^{-1}), 3423, 3092(C-$H_{aromatic}$), 2962(C-$H_{aliphatic}$), 2931(C-$H_{aliphatic}$), 2861(C-$H_{aliphatic}$), 2593, 2231(conjug. C≡N), 1575, 1495, 1462, 1380, 1295, 1203, 1059, 936, 830, 740, 472.

2.3.2. Synthesis of 1,4,8,11,15,18,22,25-octa(2-ethylhexyloxy) phthalocyaninato nickel(II) 2

A mixture of **1** (1.54 g, 4 mmol), nickel acetate tetrahydrate (0.3 g, 1.2 mmol) and a catalytic amount of 1,8-diazabicyclo [5.4.0] undec-7-ene (DBU) was refluxed in dry 1-pentanol under argon for 6 h. After cooling, the dark green solid was filtered and washed several times with dry methanol. The crude product was purified by column chromatography on silica gel using a mixture of *n*-hexane/CH_2Cl_2 (98/2) as eluent to afford a dark green solid **2**. Yield = 0.61 g, 38%. Compound **2** is soluble in $CHCl_3$, THF, ethyl acetate, DMF and DMSO. Melting point (DSC): 47.9 °C. Anal. Calc. for $C_{96}H_{144}N_8O_8Ni$ (1596.92 g mol^{-1}): C, 72.20; H, 9.09; N, 7.02; Ni, 3.67. Found: C, 70.95; H, 9.70; N, 6.88; Ni, 3.44. MS (LCQ-MS, MeOH/THF): *m/z* 1600 $(M+4H)^+$. IR (KBr pellets) ν_{max} (cm^{-1}), 3355, 3050(C-H arom.), 2960(C-$H_{aliphatic}$), 2924(C-$H_{aliphatic}$), 2852(C-$H_{aliphatic}$), 1605(C=$C_{aromatic}$), 1506, 1461, 1379, 1264, 1219, 1102(C-O-C), 1030, 923, 797, 735, 617, 465. UV–Vis

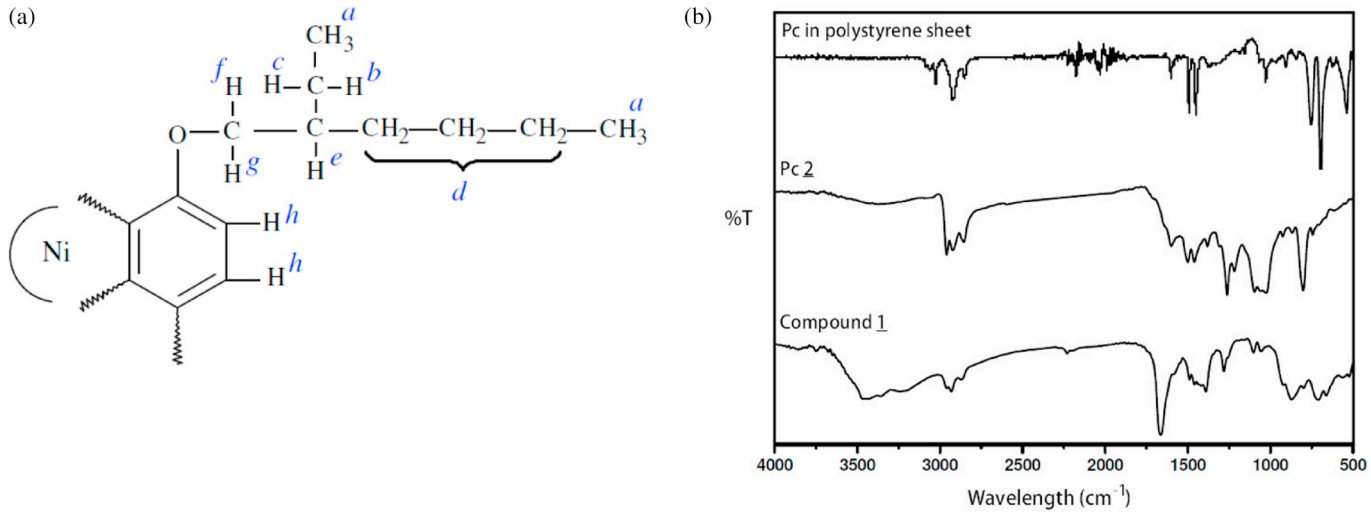

Fig. 1. a. ^{1}H NMR Prediction of the expected structure of the Ni-phthalocyanine complex. **b.**FTIR spectra of phthalocyanine precursor 1, phthalocyanine 2 and phthalocyanine-doped polystyrene sheet.

($CHCl_3$), λ_{max} (nm): 743, 665, 293, 243.

^{1}H NMR spectra of phthalocyanine **2** in $CDCl_3$ shows the expected patterns for the proposed structure: δ = 0.89 [m, 24H(*a*)], 1.11 [m, 4H (*b*)], 1.23 [m, 4H(*c*)], 1.39 [m, 24H(*d*)], 1.64 [m, 4H(*e*), 3.49 [t, 4H(*f*)], 3.92 [t, 4H(*g*)], 8.90 [m, 8H(*h*)], Fig. 1a.

2.3.3. Preparation of mono-dispersed polystyrene nanospheres

The cationic polystyrene nanospheres (PS) were prepared by emulsifier-free emulsion polymerization [14] with slight modification. A mixture of styrene (10.0 g), PVP (1.5 g), AIBA (0.26 g), and H_2O (100.0 g) were put into a 250 mL three-neck round-bottom flask equipped with a thermometer and a nitrogen inlet. The flask was placed in an ice bath and mixture was then subjected to a supersonic mixing (400 W) for 10 min. A mechanical stirrer and Graham condenser were then placed on the set. The solution was deoxygenated by bubbling argon gas for 30 min and then reacted at 70 °C for 8 h at the stirring rate of 200 rpm. Purification of the prepared polymer was achieved by dialysis versus ethanol using a cellulose membrane.

2.3.4. Fabrication of fluorophore doped polystyrene sheets

Phthalocyanine-doped polystyrene films were prepared by casting a solution of 30% (W/V) polystyrene in THF and phthalocyanine **2** onto non-luminescence glass slides. The concentration of phthalocyanine **2** in PS was approximately 4.0×10^{-5} mol L^{-1}. The films were dried at room temperature under reduced pressure and stored in the dark till use. Thickness of the films was determined by use of a micron-sensitive caliper.

2.4. Sample preparation

All samples were collected between October 2016 and Jan 2018 from the New Al-Kasr-EL-Aini Teaching Hospital Cairo University and Ain Shams Specialized Hospital, Ain shams University, Cairo, Egypt. After a standard history and physical examination, blood was drawn for routine laboratory measures. Serum samples were collected from all the volunteers; (i) control subjects (4 samples), (ii) patients ovarian cancer (6 samples). 3.0 mL of citrate solution was added to 4.0 mL plasma and the solution was centrifuged for 15.0 min at 4000 rpm to remove all proteins. After decantation, 1.0 mL of the serum was added with 0.1 mL of the buffer (pH = 7.3) to the thin film nano optical biosensor in the cuvette, and finally the 1.9 mL of water was added to give the test solution.

2.5. Proposed method

An appropriate amount (100 μL) of various standard concentrations of the CA-125 in water was mixed with the thin film doped nano nickel (II)phthalocyanine in the cell. The luminescence spectra were then recorded at the $\lambda_{ex}/\lambda_{em}$ = 685/790 nm. The optical biosensor was rinsed with water after each measurement and the calibration plot was constructed by plotting (F_0/F -1) at λ_{em} = 790 nm on the y axis against the CA-125 concentration on the x axis. The concentration of CA-125 was measured by withdrawing (100 μ L) of each serum sample and diluted to 3 mL by water in cell of the spectroflurometer in presence of the biosensor and then the emission intensity of the optical biosensor was measured at 790 nm.

2.6. Standard method

The ADVIA Centaur CP CA 125 II assay is a two-site sandwich immunoassay using direct chemiluminometric technology, which uses two monoclonal mouse antibodies specific for CA 125. The first antibody is directed toward the M11 antigenic domain, and is labeled with acridinium ester. The second antibody is directed toward the OC 125 antigenic domain and is labeled with fluorescein. The immune complex formed with CA 125 is captured with monoclonal mouse anti-fluorescein antibody coupled to paramagnetic particles in the Solid Phase.

2.7. Method validation

2.7.1. Dynamic range

The dynamic range was obtained from the effect of the concentration of the CA-125 on the luminescence intensity of the optical biosensor thin film NiPc **2** doped PS matrix. The Stern-Völmer equation was applied for the relation between the CA-125 concentrations and the luminescence intensity of the optical biosensor, $(\mathbf{F_0/F)-1} = \kappa_{sv}\,[Q]$. Where, F_o and F are the luminescence intensities of the optical biosensor in absence and in presence of the CA-125, respectively, [Q] is the concentration of the CA-125, and κ_{sv} is called Stern-Völmer constant. The slope of the fitted data is equal to the Stern-Völmer constant and one over κ_{sv} equals $C_{1/2}$ (half quenching concentration) and R_0 is critical transfer distance, which is the average distance between the donor and the acceptor, at which the probability of intermolecular energy transfer is just equal to the sum of probabilities for all the de-excitation processes of the donor excited state, $R_o = 7.35/(C_{1/2})^{1/3}$, if R_o less than 10 Å this means that the quenching is carried out by static mechanism in which the electron transfer from the optical biosensor to the quencher

(CA-125), while if R_o has a value more than 10 Å this means that the quenching is carried out by dynamic mechanism. The detection limit (LOD) and quantification detection limits were calculated according to ICH guidelines using the formulae: LOD = 3.3 S/b and LOQ = 10 S/b, (where S is the standard deviation of blank luminescence intensity values, and b is the slope of the calibration plot).

2.7.2. Accuracy and precision of the method

To evaluate the accuracy and precision, the assays described under general procedures were repeated three times within the day to determine the repeatability (intra-day precision) and three times on different days to determine the intermediate precision (inter-day precision) of the method. These assays were performed for four control serum samples and serum samples of the six patients have ovarian cancer disease. Accuracy was evaluated as percentage relative error (RE) between the measured mean concentrations and the taken concentrations of CA-125. Bias {bias % = [(Concentration found - known concentration) × 100 / known concentration] was calculated at each concentration.

3. Results and discussion

3.1. Synthesis of the fluorescent phthalocyanine 2

A novel near infrared-fluorescent polymeric thin film was prepared by impregnating a new non-peripherally octa substituted nickel(II) phthalocyanine into polystyrene. The structure of the prepared phthalocyanine fluorophore was determined using liquid chromatography quadrupole-ion mass spectroscopy (LCQ-MS), atomic absorption spectroscopy (AAS), FTIR, UV–Vis, and elemental analysis. Impregnation of this phthalocyanine onto polystyrene followed by solvent casting technique produced a monolithic thin film of high fluorescence in the near infrared region. The NIR-fluorescent materials are significant in that their absorbance far from the visible region where the biological molecules mostly absorb [15]. NIR dyes are of great current interest in chemical biology because they allow for imaging with minimal auto fluorescence from biological samples, reduced light scattering, and high tissue penetration [10]. Non-peripheral substituted phthalocyanines are known for their near infrared (NIR) absorption and emission properties and often applied for fluorescence sensing and imaging of solid tumors [16]. In this work, we have utilized the well-known Base catalyzed nucleophilic substitution of the nitro-phthalonitrile [17,18] for preparation of a novel NIR fluorescent non-peripherally octa substituted phthalocyanine **2**, Scheme 1. The non-peripheral substitution with the eight ethylhexyl groups affords not only NIR fluorescence but also a high solubility in the most of organic solvents such as THF and chloroform and this facilitate the processing of the dye in the polymer matrix using solvent casting method.

3.2. Characterization of phthalocyanine 2

FTIR spectrum of the prepared phthalocyanine precursor **1** (Fig. 1b) indicated the presence of characteristic stretching vibrations of the aromatic C—H bond (ν = 3092 cm^{-1}), the aliphatic C—H bonds in ethylhexyl group residue(ν = 2962, 2931 and 2861 cm^{-1}) and the conjugated nitrile group (ν = 2231 cm^{-1}). IR spectrum of **2** (Fig. 1b) was consistent with the assigned structure. IR spectrum shows the expected absorptions such as $\nu_{C=Carom.}$ at 1605 cm^{-1}, stretching vibrations of the aromatic C—H bond (ν = 3050 cm^{-1}), the aliphatic C—H bonds in ethylhexyl group residue(ν = 2960, 2924 and 2852 cm^{-1}) and the ether group (C-O-C) at 1102 cm^{-1}) [19]. The cyclization of **1** into phthalocyanine **2** is further confirmed by the absence of the stretching vibration of the cyano group at 2231 cm^{-1}. The absence of the N-H vibration at 700 cm^{-1} in the IR spectrum of **2** rules out the formation of metal-free *Pc* [20]. The broad peak at 3410 cm^{-1} is attributed to OH resulting from the adsorped moisture [21].

The ground state electronic absorption spectra of phthalocyanine **2** (Fig. 2a) showed the characteristic absorption patterns of a metal-phthaocyanine. In THF, the main Q band component was present at λ_{max} = 743 nm due to the transition from (a_{1u}) to (eg) molecular orbitals [21]. The small band at λ_{max} = 665 nm has been often referred to as the X band appearing as a result of deformation of the phthalocyanine ring in some solvents [22]. The Q band of the non-peripheral octa-substituted nickel-phthalocyanine **2** is red-shifted (743 nm) when compared to the corresponding peripheral substituted nickel-phthalocyanine [23]. This red spectral shift is typical of non-peripherally substituted phthalocyanines and is attributed to linear combinations of the atomic orbitals (LCAO) coefficients at the non-peripheral positions of the Highest Occupied Molecular Orbital (HOMO)(a_1u) being greater than those at the peripheral positions [24]. As a result, the HOMO (a_1u) level is destabilized more at the non-peripheral position that it is at the peripheral position. Essentially, the energy gab (ΔE) between the HOMO and Lowest Unoccupied Molecular Orbital (LUMO)*(eg)* becomes smaller, resulting in a bathochromic shift [25]. The shoulder between 400 and 500 nm may be due to charge transfer from the electron-rich ring (a_2u), (b_2u) molecular orbitals to the electron-poor metal *(a1g)*, *(b1g)* molecular orbitals, respectively (Fig. 2b), [22].

3.3. Preparation of Pc-polystyrene fluorescent films

In this work, polystyrene was prepared and used as a substrate for incorporating the phthalocyanine fluorescent molecules. Incorporation

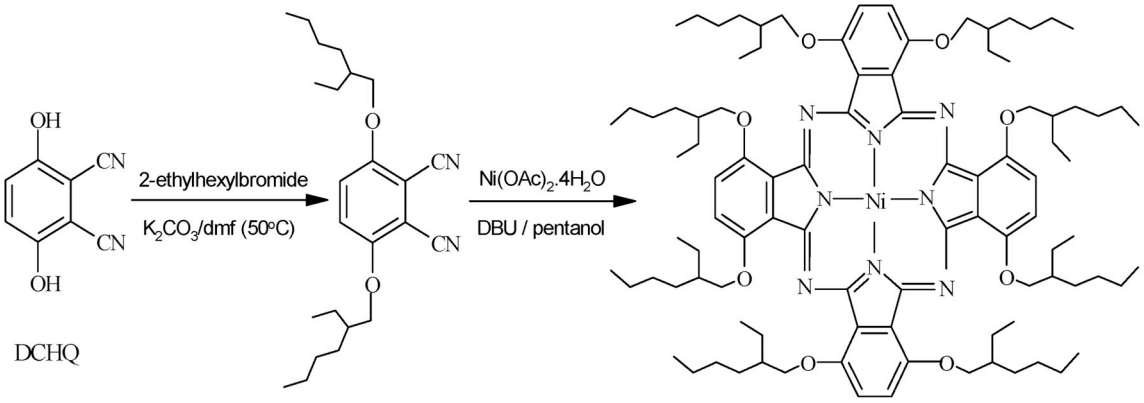

Scheme 1. Preparation of phthalocyanine precursor **1** and phthalocyanine **2**.

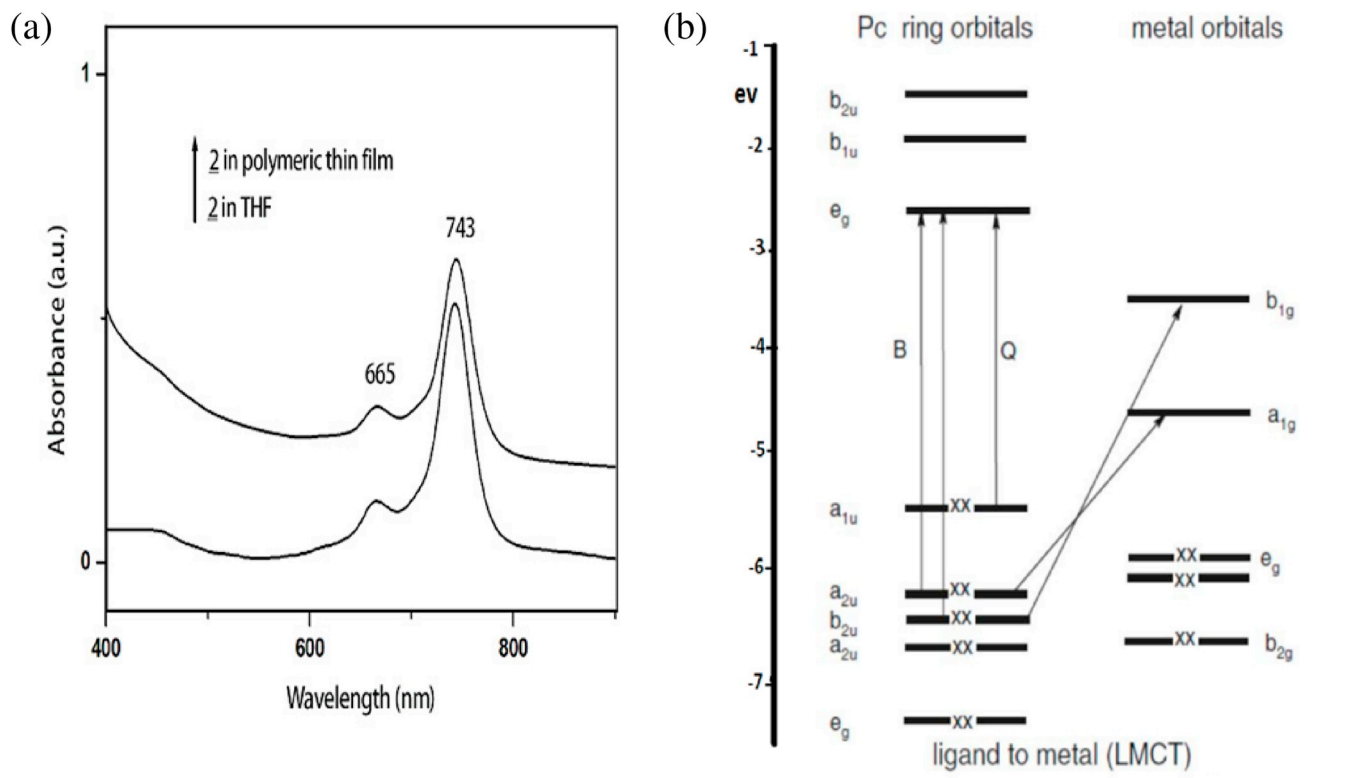

Fig. 2. a. Visible region absorption spectra of NiPc2in THF (dotted) and in the polymeric thin film (solid). **b.** Charge transfer pathway from PC to metal molecular orbitals.

of the highly photo sensitive phthalocyanine in a polymer matrix allows for an ease application as a medical kit and enhances the photo stability of the sensor material. Mono-dispersed cationic polystyrene nanoparticles were prepared by emulsifier-free emulsion polymerization using PVP as the stabilizer and AIBA as the cationic initiator. Emulsifier-free emulsion polymerization is the most convenient method for preparation of mono-dispersed biocompatible polystyrene suitable for biomedical applications [16]. XRD and TEM measurements of *Pc*-polymer sheets were showed in **S. Date 1 and 2**. DLS measurements showed mono-dispersed nano spheres of average hydrodynamic diameter (D_h) of 240 ± 2.1 nm. The zeta-potential measurements showed that the polymeric nano spheres have a positive potential of about 32 ± 2.6 mV. GPC measurements of the prepared polymer showed monodispersed polymeric species ($M_w = 230 \times 10^3$ g mol^{-1}, $M_n = 185 \times 10^3$ g mol^{-1}, Mw/Mn = 1.24). FTIR spectrum (Fig. 1b), of the prepared polymer is consistent with the spectra known for polystyrene specially the aromatic CH stretching vibration (3030-3080 cm^{-1}) [26,27]. Casting of *Pc*-PS in THF affords monolithic films of good mechanical properties.

3.4. Characterization of Pc-polystyrene fluorescent films

The ground state electronic absorption spectra of **2** in solution and in the prepared polymeric sheets are shown in (Fig. 2a). The shape of the spectra is almost the same, indicating that there is no interaction between NiPc**2** and polystyrene in the energetically ground state. The spectra demonstrate the monomerization (disaggregation) of the phthalocyanine molecules in the polymeric sheets and this is an important feature for an efficient optical sensor. Neither broadening nor blue shift of the main Q-band of the phthalocyanine were observed when impregnated in the polymeric sheets (Fig. 2a) and this evidences the high dispersion of the *Pc* molecules in the polymeric matrix [27].

AFM image of the prepared fluorescent thin film (Fig. 3a) gives a detailed information about the surface morphology and homogeneity of the thin film doped nickel(II)phthalocyanine nanoparticles. The surface roughness of the thin film doped nanonickel(II)phthalocyanineis 89.43 nm. The interface roughness decreases when thin film doped nickel(II)phthalocyanine nanoparticles is assembled into the PS matrix. In addition, a vertical grain structure of the multilayer surface can be observed from three-dimensional AFM images which show that the distribution of aggregated clusters is almost uniform, (Fig. 3a). Fluorescence measurements of the prepared fluorescent thin film are shown in **S. Data 3.** The fluorescence emission bands at 712 and 790 nm of the Ni-*Pc* embedded in the PS sheet are attributed to the electron transfer from the HOMO (a_1u) mainly *Pc* character to LUMO (b_1g) mainly Nickel metal ion character, then relaxation from the b1g energy state of the metal ion to a1u energy state of *Pc*. The fluorescence emission spectrum of the thin film NiPc2 doped PS matrix at λ_{ex} = 685 nm is displayed in (Fig. 3b). The intensity of this fluorescence peak at 790 nm was decreased in the presence of different concentrations of CA-125 protein, (Fig. 3b).

The 3d orbitals of Ni are considerably lower in energy, when compared with *Pc* orbitals. As a result, the occupied 3d-like orbitals lie significantly below the *Pc* (a1u) molecular orbital, making the latter the HOMO of the system. The 3dπ participation in (2eg) molecular orbitalis diminished in Ni ion. The empty 3d-like (b1g) molecular orbital (dx2-y2) lies just beneath 2eg. The one-electron excitation occurs from the (a1u) HOMO to (2eg) LUMO. In the presence of CA-125 as ligand attacks Ni metal ion in Ni-*Pc* complex from below and above of axial positions through its An N-terminal domain (polar glycosylated tail), in which a sugar molecule is attached to an oxygen atom in an amino acid residue in a protein. the molecular geometry of Ni-*Pc* is changed from square planar shape to distorted octahedral shape. This change in the geometry leads to the first electron from CA-125 is added to the (1e g) (p) orbital of *Pc*, leaving (b1g)(dx2-y2) unoccupied.

Addition of electrons to (2e g) of Ni ion raises the energy of (b1g) of Ni ion, placing the latter above the former. In this case (2e g) and (b1g) represent the HOMO and LUMO, respectively, in Ni-*Pc* –CA 125

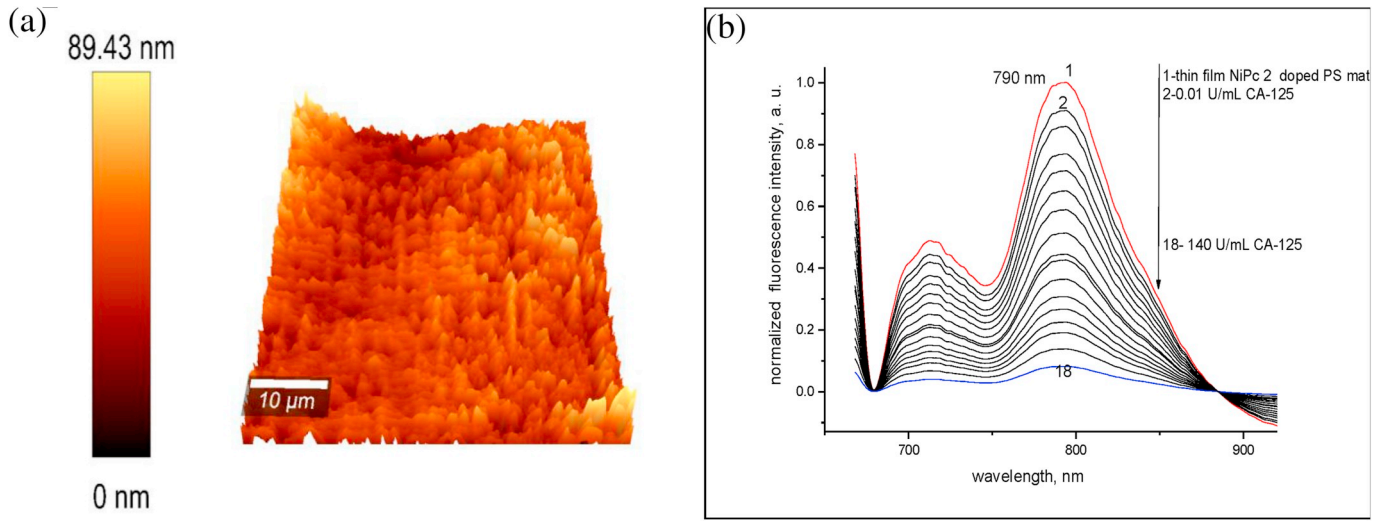

Fig. 3. a. AFM image of phthalocyanine-doped polystyrene sheet. **b.** Fluorescence emission spectra of the thin film NiPc 2 doped polystyrene matrix in different concentration of CA-125 protein at λex = 685 nm.

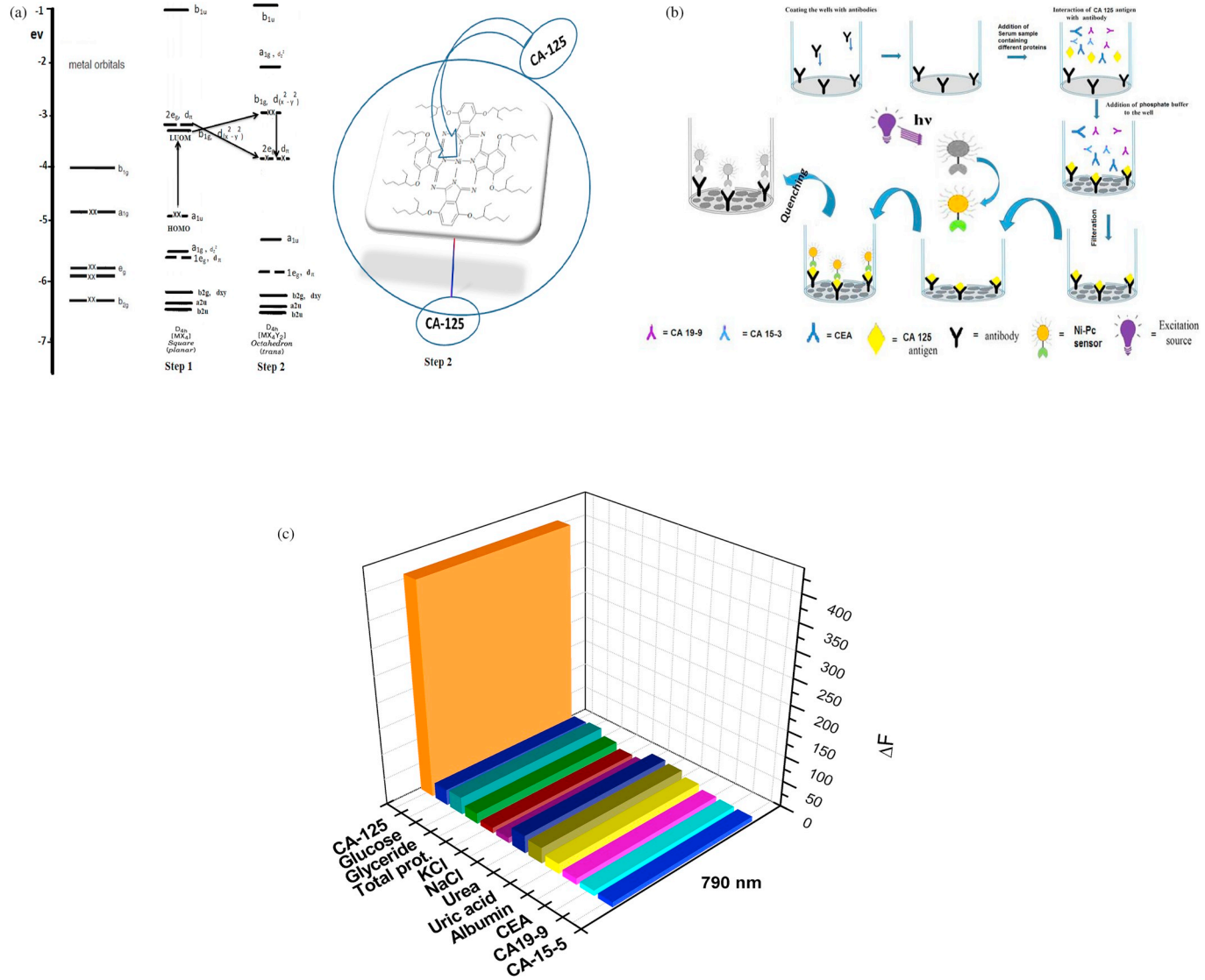

Fig. 4. a. Molecular orbital energy diagrams of Ni-*Pc* and Ni-*Pc*-CA 125. hν. **b.** Reaction of CA-125 with its antibody. **c.** Effect of interfering species on the luminescence intensity of the optical sensor.

complex. In this case the ground state (HOMO) and excited state (LUMO) have metal ion character this leads to the quenching of the fluorescence intensity of the Ni-*Pc* complex in presence of CA-125 (Fig. 4a), [28].

3.5. Analytical parameters

It is known that solvents have a significant effect on the luminescence intensity of phthalocyanines. This effect on NiPc@PS nanocomposites was investigated in this study. Protic solvents such as ethyl alcohol and water were found to increase the luminescence intensity, whereas a significant decrease of the intensity was observed in aprotic solvents. This is attributed to the fact that aprotic solvents destabilizes the excited state of the fluorophore [29–41]. The influence of CA-125 concentration on the luminescence intensity of the thin film NiPc **2** doped PS was studied under the optimum experimental conditions and the results are shown in (Fig. 3b). The luminescence intensity of the thin film NiPc **2** doped PS matrix was quenched by increasing the concentration of CA-125 to 130 U mL^{-1} (Fig. 3b). The tolerable limit was defined as the concentration of the added species individually causing a deviation less than 3% of the luminescence intensity at the optimum conditions of the optical biosensor the thin film NiPc **2** doped PS matrix. Fig. 4b shows that the separation of CA 125 from other interfering protein the serum sample. From the ΔF values the interfering species have not significant effect on the luminescence intensity of the thin film NiPc **2** doped PS matrix with CA-125, (Fig. 4c).

3.6. Method validation

3.6.1. Dynamic range

From the Stern-Völmer plot of [(F_0/F)-1] against [CA-125] [42], the luminescence intensity at 790 nm is decreased linearly with the concentrations of CA-125 over the range 1.0 × 10^{-2} -127 U mL^{-1} with a correlation coefficient of 0.99, (Fig. 5), Table 1. The detection limit (LOD) and quantification detection limits were calculated according to ICH guidelines [43] are also presented in Table 1. The comparison of the proposed nano optical biosensor for the determination of CA-125 with other published methods [44–52] indicate that the developed method has good stability, lower limit of detection (1.0 × 10^{-4} U mL^{-1}) and wide linear range of application (1.0 × 10^{-2} −127 U mL^{-1}).

3.6.2. Accuracy and precision of the method

To evaluate the accuracy and precision, the assays described under general procedures given in the experimental part. The results of this study are given in Table 2. The percentage relative standard deviation

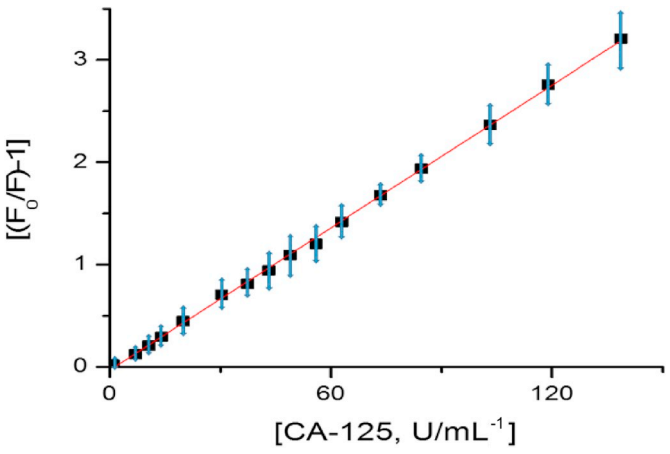

Fig. 5. Fitting of Stern-Völmer equation for Fluorescence emission spectra of thin film nano Ni-*Pc* embedded in PS sheet in different concentrations of CA-125 at λ_{ex} = 685 nm.

Table 1
Sensitivity and regression parameters for the proposed method.

value	Parameter
790	λ_{em} nm
10^{-2} - 127	Linear range, U mL^{-1}
10^{-4}	Limit of detection (LOD), U mL^{-1}
3.3 × 10^{-4}	Limit of quantification (LOQ), U mL^{-1}
Y = a + bX	Regression equation, Y[a]
0.001	Intercept (a)
0.023	Slope (b)
0.01	Standard deviation
1.0	Variance (Sa^2)x 10^{-4}
0.9	Regression coefficient (r)

[a] Where Y = fluorescence intensity, X = concentration in n mol L^{-1}, a = intercept, b = slope.

(%RSD) values were ≤ 1.01–3.60 (serum) (intra-day), ≤ 1.30–3.50 % (serum) (inter-day) indicating the high precision of the method. Accuracy was evaluated as percentage relative error (RE) between the measured mean concentrations and the taken concentrations of CA-125 (Table 2). Percent relative error (% RE) values of ≤ 0.35–5.55 % (serum) (intra-day) and ≤ 1.42–6.66 % (serum) (inter-day) demonstrates the high accuracy of the proposed method. The *F* and *t* tests of the obtained results at 95% confidence level did not exceed the theoretical ones without significant differences between the developed and the standard methods confirming the accuracy of the developed procedure, Table 2.

3.7. Application

Cancer Antigen 125 is a protein that is mostly overexpressed in the blood of ovarian cancer patients and this helps to design an efficient diagnostic tool of ovarian cancer.

This protein is performed on the surface of the malignant cells and diffused in the blood stream. Elevated levels of CA-125 were reported in more than 80 percent of women with late-stage ovarian cancer, and in 50 percent of early-stage patients. The analytical utility and applicability of the method proposed in this work was investigated by observing CA-125 concentration in various serum samples (5 samples) of health state and (10 patients) ovarian cancer in the range of age (30y – 65y). The average values obtained by the given method (12.1–29.5 ± 1.42–3.6 U mL^{-1}), (77.4–234 ± 1.02–3.1 U mL^{-1}) match well with the values obtained by the standard method (12–29 ± 1.42–2.1 U mL^{-1}), (77-230 ± 0.88–2.87 U mL^{-1}) for serum samples of heath state and ovarian cancer, respectively, Table 2.

4. Conclusions

The developed method provides an excellent approach for measuring CA-125 as a good biomarker for early diagnosis of ovarian cancer disease. The CA-125 was determined by the thin film Ni-Pc doped in PS matrix. The method is sensitive and provides a wide linear dynamic range of CA-125 concentrations by measuring the fluorescence intensity of thin film Ni-Pc doped in PS matrix under the optimal conditions. A detection limit of 1.0 10^{-4} U mL^{-1} was accomplished.

Acknowledgments

This project was funded by the Deanship of Scientific Research (DSR), University Of Jeddah, Jeddah, under grand No. (G-1436-965-568). The authors, therefore, acknowledge with thanks DSR technical and financial support.

Table 2
Evaluation of intra-day and inter-day accuracy and precision of the proposed method in case of different serum samples.

Proposed method																Standard method			Serum sample
Inter day precision				Intraday precision				F-test	*t*-test	Recovery%	RSD%	Average	Readings			RSD%	±	Average	
RSD%	RE%	CL	Average Reading	RSD%	RE%	CL	Average Reading												
2.5	0.8	0.5	12.3	2.2	0.8	0.4	12.1	1.0	0.1	99.2	2.2	12.1	11.5	12.7	12.2	2.2	±	12.2	1
1.7	2.2	0.7	26.8	1.5	0.7	0.6	26.4	1.6	0.5	100.7	1.5	26.4	27.2	26.7	25.5	1.8	±	26.2	2
1.9	3.4	0.9	30.1	1.7	1.3	0.8	29.5	0.9	0.6	101.3	1.7	29.5	30.6	28.5	29.6	1.7	±	29.1	3
4.3	3.7	1.3	19.2	3.9	2.7	1.1	19.0	0.3	1.9	102.7	3.8	19.0	18.0	20.0	19.0	2.2	±	18.5	4
1.2	2.5	2.1	112.0	1.1	0.3	1.8	109.6	0.8	0.1	100.3	1.0	109.6	109.6	110.6	108.8	0.9	±	109.2	5
2.5	2.2	4.6	116.0	2.3	0.2	4.0	113.7	1.0	0.1	100.2	2.2	113.7	115.0	114.0	112.0	2.2	±	113.4	6
3.5	2.0	6.1	106.0	3.2	0.7	5.3	104.7	0.9	0.1	100.7	3.1	104.7	103.0	107.0	106.0	2.9	±	103.9	7
3.1	1.2	10.	201.0	2.9	0.2	8.9	199.0	1.0	0.1	100.2	2.8	199.0	201.0	196.0	200.0	2.7	±	198.5	8
3.7	1.3	11.5	192.0	3.4	0.2	10.0	190.0	0.9	0.1	100.2	3.2	190.0	191.0	187.0	192.0	3.1	±	189.5	9
2.5	2.1	9.6	237.0	2.3	0.8	8.3	234.0	0.9	0.4	100.8	2.3	234.0	237.0	234.0	231.0	2.3	±	232.0	10

%RE. Percent relative error, %RSD. relative standard deviation and CL. Confidence limits were calculated from: CL = ± tS/√n. (The tabulated value of t is 4.303, at the 95% confidence level; S = standard deviation and n = number of measurements). Theoretical values of t- and f-tests at 95% confidence limits are 4.303 and 19.0, respectively.

Appendix A. Supplementary data

Supplementary data to this article can be found online at https://doi.org/10.1016/j.talanta.2019.03.119.

References

[1] S.E. Mackey, W.T. Creasman, Ovarian cancer screening, J. Clin. Oncol. 13 (1995) 783–793.
[2] M.K. Schwartz, Cancer markers, in: V.T. DeVita, S. Hellman, S.A. Rosenberg (Eds.), Cancer: Principles and Practice of Oncology, JB Lippincott company, Philadelphia, 1993, p. 534 1993.
[3] P.T. Lavin, R.C. Knapp, G. Malkasian, et al., CA 125 for the monitoring of ovarian carcinoma during primary therapy, Obstet. Gynecol. 69 (1987) 223–227.
[4] J.A. Ledermann, F.A. Raja, C. Fotopoulou, A. Gonzalez-Martin, N. Colombo, C. Sessa, Newly diagnosed and relapsed epithelial ovarian carcinoma: ESMO Clinical Practice Guidelines for diagnosis, treatment and follow-up, Ann. Oncol. 24 (2013) 24–32.
[5] American Congress of Obstetricians and Gynecologists, "Five Things Physicians and Patients Should Question" (http://www.choosingwisely.org/doctor-patient-lists/american-college-of-obstetricians-and-gynecologists/), Choosing Wisely: an Initiative of the ABIM Foundation, American Congress of Obstetricians and Gynecologists, (Retrieved 1,August 2013).
[6] D. Gupta, C.G. Lis, Pretreatment serum albumin as a predictor of cancer survival: a systematic review of the epidemiological literature, Nutr. J. 9 (2010) 69–74.
[7] R.C. Bast, T.L. Klug, E. St John, E. Jenison, J.M. Niloff, H. Lazarus, R.S. Berkowitz, T. Leavitt, C.T. Griffiths, L. Parker, V.R. Zurawski, R.C. Knapp, A radioimmunoassay using a monoclonal antibody to monitor the course of epithelial ovarian cancer, N. Engl. J. Med. 309 (1983) 883–887.
[8] P. Gözce, H. Vahrson, Significance of determination of squamous cell carcinoma antigen in the follow up of patients with cancer of the uterine cervix, Orv. Hetil. 134 (1993) 915–918.
[9] A. Santillan, R. Garg, M.L. Zahurak, G.J. Gardner, R.L. Giuntoli, D.K. Armstrong, R.E. Bristow, Risk of epithelial ovarian cancer recurrence in patients with rising serum CA-125 levels within the normal range, J. Clin. Oncol. 23 (2005) 9338–9343.
[10] K.M. Kadish, K. Smith, M.R. Guilard, The Porphyrin Handbook vol. 20, Elsevier Science, San Diago, California, USA, 2003.
[11] S. Luo, E. Zhang, Y. Su, T. Cheng, C. Shi, A review of NIR dyes in cancer targeting and imaging, Biomaterials 32 (2011) 7127–7138.
[12] P. Khoza, T. Nyokong, Visible light transformation of Rhodamine 6G using tetra-carbazole zinc phthalocyanine when embedded in electrospun fibers and in the presence of ZnO and Ag particles, J. Coord. Chem. 68 (2015) 1117–1131.
[13] A.B. Sorokin, Phthalocyanine metal complexes in catalysis, Chem. Rev. 113 (2013) 8152–8191.
[14] B.L. Wheeler, G. Nagasubramanian, A.J. Bard, L.A. Schechtman, D.R. Dininny, M.E. Kenney, A silicon phthalocyanine and a silicon naphthalocyanine: synthesis, electrochemistry, and electrogenerated chemiluminescence, J. Am. Chem. Soc. 106 (1984) 7404–7410.
[15] A.C.S. Lobo, A.D. Silva, V.A. Tomé, S.M.A. Pinto, E.F.F. Silva, M.J.F. Calvete, C.M.F. Gomes, M.M. Pereira, L.G.J. Arnaut, Phthalocyanine labels for near-infrared fluorescence imaging of solid tumors, Med. Chem. 59 (2016) 4688–4696.
[16] Y. Amao, K. Asai, I. Okura, Fluorescence quenching oxygen sensor using an aluminum phthalocyanine–polystyrene film, Anal. Chim. Acta 407 (2000) 41–44.
[17] W.M. Darwish, N.A. Bayoumi, M.T. El-Kolaly, Laser-responsive liposome for selective tumor targeting of nitazoxanide nanoparticles, Eur. J. Pharm. Sci. 111 (2018) 526–533.
[18] M. Durmus, M.M. Ayhan, A. GülGürek, V. Ahsen, Peripherally alpha(α)-substituted novel phthalocyanines, Dyes Pigments 77 (2008) 570–577.
[19] W.M. Darwish, A.M. Darwish, E.A. Al-Ashkar, Synthesis and nonlinear optical properties of a novel indium phthalocyanine highly branched polymer, Polym. Adv. Technol. 26 (2015) 1014–1019.
[20] W.M. Darwish, E. Seikel, R. Kasmarker, K. Harms, J. Sundermeyer, Synthesis and X-ray crystal structures of imido and ureato derivatives of titanium(IV) phthalocyanine and their application in the catalytic formation of carbodiimides by metathesis from isocyanates, Dalton Trans. 40 (2011) 1787–1792.
[21] D. Ximing, X. Huijun, The synthesis and film-forming property of a new amphiphilic phthalocyanine, Dyes Pigments 39 (1998) 223–229.
[22] Q. Zhang, Y. Han, W. Wang, T. Zhang, J. Chang, Preparation of fluorescent polystyrene microspheres by gradual solvent evaporation method, Eur. Polym. J. 45 (2009) 550–556.
[23] F. Yuksel, M. Durmus, V. Ahsen, Photophysical, photochemical and liquid-crystalline properties of novel gallium(III) phthalocyanines, Dyes Pigments 90 (2011) 191–200.
[24] H. Konami, M. Hatano, A. Tajiri, Inter-ring overlap integrals in dimer complexes of phthalocyanines and porphyrins, Chem. Phys. Lett. 166 (1990) 605–608.
[25] K. Hanson, L. Roskop, P.I. Djurovich, F. Zahariev, M.S. Gordon, M.E. Thompson, A paradigm for blue- or red-shifted absorption of small molecules depending on the site of π-extension, J. Am. Chem. Soc. 132 (2010) 16247–16255.
[26] P. Huhtinen, M. Kivelä, T. Soukka, H. Tenhub, T. Lővgrena, H. Härmä, Preparation, characterisation and application of europium(III) chelate-dyed polystyrene–acrylic acid nanoparticle labels, Anal. Chim. Acta 630 (2008) 211–216.
[27] T. Basova, E. Kol'tsov, A.K. Ray, A.K. Hassan, A.G. Gurek, V. Ahsen, Liquid crystalline phthalocyanine spun films for organic vapour sensing, Sens. Actuators, B 113 (2006) 127–134.
[28] S.L. Meng, S.J. Steve, Electronic structure and bonding in metal phthalocyanines, Metal = Fe, Co, Ni, Cu, Zn, Mg, Chem. Phys. 114 (2001) 9780–9791.
[29] A.E. Amr, M.S. Attia, Novel application of pyronin Y fluorophore as high sensitive optical sensor of glucose in human serum, Talanta 107 (2013) 18–24.
[30] M.S. Attia, A.O. Youssef, R.H. El-Sherif, Durable diagnosis of seminal vesicle and sexual gland diseases using the nano optical sensor thin film Sm-doxycycline complex, Anal. Chim. Acta 835 (2014) 56–64.
[31] M.S. Attia, A.O. Youssef, A.E. Amr, Europium-sensitized and simultaneous pH-assisted spectrofluorimetric assessment of ciprofloxacin, norfloxacin and gatifloxacin in pharmaceutical and serum samples, J. Photochem. Photobiol. A Chem. 236 (2012) 26–34.
[32] M.S. Attia, A.O. Youssef, A.M. Othman, E. El-Raghi, Excited state interaction between Hydrochlorothiazide and europium ion in PMMA polymer and its application as optical sensor for Hydrochlorothiazide in tablet and serum samples, J. Lumin. 132 (2012) 2049–2053.
[33] M.S. Attia, M.N. Ramsis, L.H. Khalil, S.G. Hashem, A highly selective and sensitive spectrofluorimetric method for the assessment of chlorzoxazone and ibuprofen in pharmaceutical formulations by using Eu-tetracycline HCl optical sensor doped in sol-gel matrix, J. Fluoresc. 22 (2012) 779–788.
[34] M.S. Attia, A.O. Youssef, A.E. Amr, M.S. Mostafa, Determination of ofloxacin using a highly selective photo probe based on the enhancement of the luminescence intensity of $Eu3^{+}$—ofloxacin complex in pharmaceutical and serum samples, J. Fluoresc. 22 (2012) 557–564.
[35] M.S. Attia, A.O. Youssef, W.H. Mahmoud, M.S. Mostafa, Cilostazol determination by the enhancement of the green emission of $Tb3^{+}$ optical sensor, J. Fluoresc. 21 (2011) 2229–2235.
[36] M.S. Attia, M.N. Ramsis, L.H. Khalil, S.G. Hashem, W.H. Mahmoud, A.M. Othman, M.S. Mostafa, Spectrofluorimetric assessment of doxycycline hydrochloride in

pharmaceutical tablets and serum sample based on the enhancement of the luminescence intensity of the optical sensor Sm3 + Ion, J. Fluoresc. 21 (2011) 1739–1748.
[37] M.S. Attia, M.M. Aboaly, Highly sensitive and selective spectrofluorimetric determination of metoclopramide hydrochloride in pharmaceutical tablets and serum samples using Eu^{3+} ion doped in sol–gel matrix, Talanta 82 (2010) 76–82.
[38] M.S. Attia, M.H. Khalil, M.S.A. Abdel-Mottaleb, M.B. Lukyanova, Yu A. Alekseenko, Boris Lukyanov, Effect of complexation with lanthanide metal ions on the photochromism of (1,3,3-trimethyl-5_-hydroxy-6_-formyl- indoline-spiro2,2_-[2H]chromene) in different media, Int. J. Photoenergy (2006) 1–9.
[39] M.S. Attia, N.S. Al Radadi, Progress of pancreatitis disease biomarker alpha amylase enzyme by new nano optical sensor, Biosens. Bioelectron. 86 (2016) 413–419.
[40] M.S. Attia, N.S. Al Radadi, Nano optical sensor binuclear Pt2pyrazinecarboxylic acid– bipyridine forenhancement of the efficiency of 3 nitrotyrosine biomarker for earlydiagnosis of liver cirrhosis with minimal hepatic encephalopathy, Biosens. Bioelectron. 86 (2016) 406–412.
[41] M.S. Attia, A.O. Youssef, Z.A. Khan, M.N. Abou-Omar, Alpha fetoprotein assessment by using a nano optical sensor thin film binuclear Pt-2-aminobenzimidazole-Bipyridine for early diagnosis of liver cancer, Talanta 186 (2018) 36–43.
[42] O. Stern, M. Völmer, About the decay time of the fluorescence, Z. Phys. 20 (1919) 183–186.
[43] International Conference on Hormonisation of Technical Requirements for Registration of Pharmaceuticals for Human Use, ICH Harmonised Tripartite Guideline, Validation of Analytical Procedures: Text and Methodology Q2(R1),Complementary Guideline on Methodology Dated 06 November 1996, Incorporated in November, London, 2005.
[44] E. Brand, Y. Lidor, The decline of CA 125 level after surgery reflects the size of residual ovarian cancer, Obstet. Gynecol. 81 (1993) 29–32.
[45] S.J. Chang, R.E. Bristow, Evolution of surgical treatment paradigms for advanced-stage ovarian cancer: redefining 'optimal' residual disease, Gynecol. Oncol. 125 (2012) 483–492.
[46] A. Elattar, A. Bryant, B.A. Winter-Roach, M. Hatem, R. Naik, Optimal primary surgical treatment for advanced epithelial ovarian cancer, Cochrane Database Syst. Rev. 8 (2011) CD007565.
[47] A. Gadducci, F. Landoni, T. Maggino, T. Sartori, E. Zola, P.A. Fanucchi, An assessment of the value of serum CA 125 measurements in the management of epithelial, Gynecol. Oncol. 63 (1996) 234–237.
[48] A. Rosen, P. Sevelda, M. Klein, J. Spona, A. Beck, A CA125 score as a prognostic index in patients with ovarian cancer, Arch. Gynecol. Obstet. 247 (1990) 125–129.
[49] G. Sölétormos, M.J. DuffyA, S. Othman, R.H. Verheijen, B. Tholander, R.C. Bast, Clinical use of cancer biomarkers in epithelial ovarian cancer: updated guidelines from the european group on tumor markers, Int. J. Gynecol. Cancer 26 (2016) 43–51.
[50] C.A. Yedema, P. Kenemans, C.M. Thomas, L.F. Massuger, T. Wobbes, R. Verstraeten, CA 125 serum levels in the early post-operative period do not reflect tumour reduction obtained by cytoreductive surgery, Eur. J. Cancer 29A (1993) 966–971.
[51] S.C. Yoo, J.H. Yoon, M.O. Lyu, W.Y. Kim, S.J. Chang, K.H.J. Chang, Significance of postoperative CA-125 decline after cytoreductive surgery in stage IIIC/IV ovarian cancer, Gynecol. Oncol. 19 (2008) 169–172.
[52] O. Zivanovic, C.S. Sima, A. Iasonos, K.M. Bell-McGuinn, P.J. Sabbatini, M.M. Leitao, Exploratory analysis of serum CA-125 response to surgery and the risk of relapse in patients with FIGO stage IIIC ovarian cancer, Gynecol. Oncol. 115 (2009) 209–214.